analytical chemistry

pubs.acs.org/ac Article

Imaging vs Nonimaging Raman Spectroscopy for High-Throughput Single-Cell Phenotyping

Alison J. Hobro,* Nicolas Pavillon, Kota Koike, Takeshi Sugiyama, Takayuki Umakoshi, Prabhat Verma, Katsumasa Fujita, and Nicholas I. Smith*

Cite This: *Anal. Chem.* 2024, 96, 7047−7055 Read Online

ACCESS | Metrics & More | Article Recommendations | Supporting Information

ABSTRACT: Raman spectroscopy can provide nonbiased single-cell analysis based on the endogenous ensemble of biomolecules, with alterations in cellular content indicative of cell state and disease. The measurements themselves can be performed in a variety of modes: generally, full imaging takes the most time but can provide the most information. By reducing the imaging resolution and generating the most characteristic single-cell Raman spectrum in the shortest time, we optimize the utility of the Raman measurement for cell phenotyping. Here, we establish methods to compare these different measurement approaches and assess what, if any, undesired effects occur in the cell. Assuming that laser-induced damage should be apparent as a change in molecular spectra across sequential measurements, and by defining the information content as the Raman-based separability of two cell lines, we thereby establish a parameter range for optimum measurement sensitivity and single-cell throughput in single-cell Raman spectroscopic analysis. While the work here uses 532 nm irradiation, the same approach can be generalized to Raman analysis at other wavelengths.

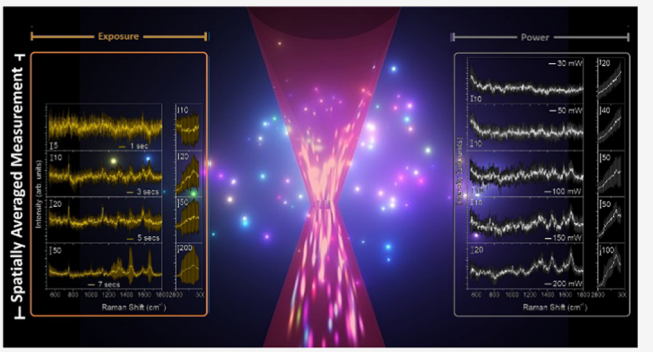

Raman spectroscopy has had wide success in the identification and analysis of samples, whether fluid, gas, or solid. Even biosamples with complex chemistry are well-suited to Raman analysis, and the label-free optical method has been able to noninvasively probe cell states, which are otherwise very difficult to measure without modification of the sample. Many cell and tissue studies have used Raman imaging (where each location in the sample is interrogated by a Raman excitation beam[1,2]) to capture spatial information, but it takes significant time to measure. However, the recent boom in single-cell sequencing studies[3] reminds us of the need for a statistically large number of samples to make sense of cell profiles, without necessarily requiring spatial resolution. Similarly, in Raman analysis, it is possible to give up spatial information in order to measure more cells and obtain the most representative spectra possible from each single cell. This can be achieved by subsampled[4] imaging to boost throughput at a reduced spatial resolution or by using only a single measurement per cell. A single spectral measurement can be a simple point targeted within the cell. It can also be performed by sweeping the beam through a significant area of the cell during a single spectral acquisition[5] or similarly by using a large focal area[6,7] or by stage scanning during each cell acquisition. Essentially, by incorporation of more of the cellular regions during a single spectral acquisition, a more comprehensive spectral evaluation of the whole cell molecular profile can be achieved while still maintaining short acquisition times. Perhaps, more importantly, any inadvertent bias resulting from the selection of the measurement region within the cell is reduced as the measurement region becomes larger.

The real limiting factor for the Raman methods mentioned stems from the need to maintain sensible levels of laser irradiation. If no laser damage occurred, we could use stronger excitation and measure all regions of the cell with shorter exposure. However, stronger excitation can produce visible cell damage if done carelessly. This can manifest immediately, e.g., as ablation[8,9] or bubbles,[10] or in less immediate ways, such as changes in cell signaling,[11−14] proliferation,[15,16] or cell blebbing.[15] The protocol for measuring Raman-based single-cell profiles should therefore be determined by the biological hypothesis being tested by the experiment, the resilience of the cell types, and the consideration of what (if any) changes in the sample are acceptable. Considerations include the expected locations of the Raman features of importance. With pertinent questions such as are these features localized to specific subcellular regions of single cells where imaging may be

Received: January 12, 2024
Revised: March 11, 2024
Accepted: March 13, 2024
Published: April 23, 2024

https://doi.org/10.1021/acs.analchem.4c00236
Anal. Chem. 2024, 96, 7047−7055

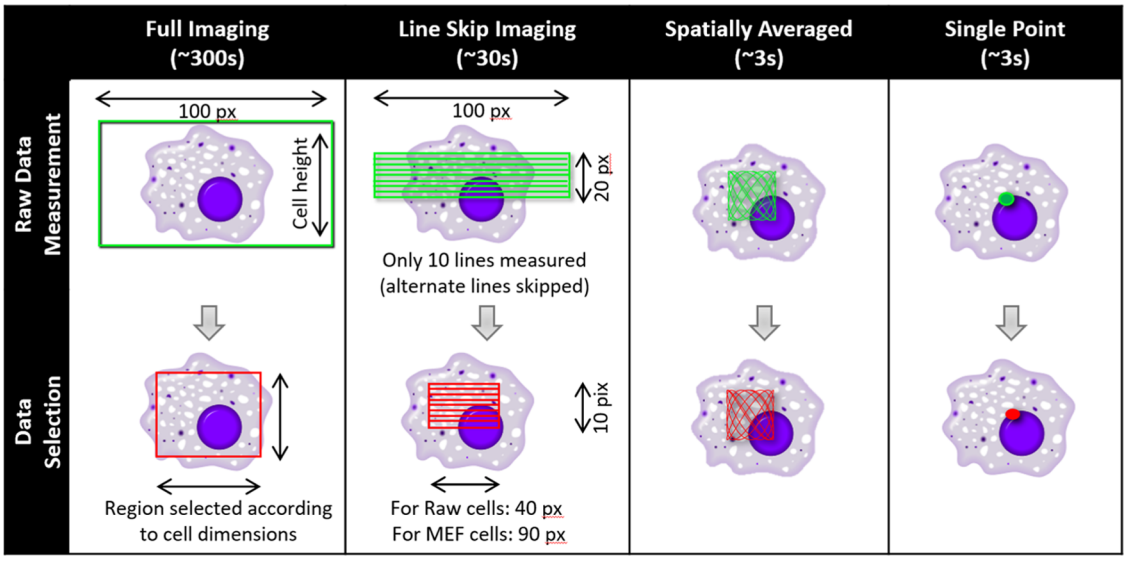

Figure 1. Overview of Raman measurement approaches to increase throughput and the corresponding data extraction used for each of the four modes discussed in this paper. Measurement regions (shown in green) are shown in the top row. The data extracted from each measurement (shown in red) are shown in the second row. Further details are given in the text. Approximate times to record one Raw 264.7 cell are given in the column headings.

required? Are all cells and tissues expected to exhibit the features of interest? If not, then a larger number of samples is needed to ensure the subpopulation is well-represented in the data. If it is necessary to study the same cell/tissue area at different time points to observe progressive processes, then minimizing any changes induced by the measurement itself would be a central consideration. The way in which the data will be later used also influences measurement protocol decisions. For example, significantly higher sample throughput is needed to robustly subtype cell populations than would be needed for exploratory measurements of whether a known phenomenon is apparent in a directly comparative Raman analysis.

Considering variability within the measurement itself, unexpected variations are an inevitable part of live cell measurement such as cell movements as a whole or rearrangement of molecules within the measurement region by active or passive processes. Bleaching of autofluorescent molecules in the cell by laser can occur but can be considered as acceptable or even advantageous since the effective Raman signal is often stronger after bleaching.[17] However, changes induced by laser irradiation of the sample, which more fundamentally modify the cell inducing a cellular response or more severe effects, such as cell blebbing or cell death, should usually be avoided. We propose a metric to quantify laser-induced change during Raman cell profiling based on simply comparing sequential measurements. While no two measurements will be identical, we can evaluate whether a repeatable change or bias occurs in the sample. Since the spectral data itself characterizes the molecular composition of the cell, we can then use spectral analysis to gain insights into which factors, if any, are consistently changing during the measurement.

Since Raman cell profiling can be performed with very different laser conditions, wavelengths, spectral range, sample throughput, resulting data formats, and other factors, there has been little previous work to compare the real-world utility of the spectral data obtained from various Raman acquisition methods. Here, we first fix the laser wavelength and spectral parameters and then explore four measurement modes: (1) full imaging, where all of a region of interest is measured; (2) line skip imaging, where a region of interest is subsampled; (3) spatially averaged measurements, where the laser irradiation is scanned across the cell during a single-point measurement; and (4) single-point measurements, where the spectrum is recorded from an isolated region within the cell. We evaluate the performance of these four methods under two criteria that can be quantified across all of the measurement types. First, how "good" are the spectra obtained, which we explicitly evaluate here in terms of the discrimination ability to identify the cell type. Second, does the measurement itself affect the sample, which we assess by the comparison of sequential measurements from the same sample. By subtracting the second measured spectrum from the first, we create a "differential spectrum" that we use to quantify the spectral change occurring during the measurement.

EXPERIMENTAL SECTION

Cell Culture. Raw 264.7 (Riken Cell Bank, Japan) and spontaneously immortalized wild-type mouse embryonic fibroblast (MEF, kindly donated by Dr. S. Akira (Osaka University, Japan)) cells were cultured in Dulbecco's modified Eagle's medium (DMEM) containing 4.5 g/L glucose, L-Gln, and sodium pyruvate (Nacalai Tesque Inc., Japan) supplemented with 10% fetal bovine serum (FBS, Gibco, Japan) and 1% penicillin−streptomycin solution (10 000 units penicillin, 10 mg/mL streptomycin, Sigma-Aldrich, Japan). Cells were plated onto poly-L-lysine (Sigma-Aldrich, Japan) coated quartz-bottomed culture dishes (FPI, Japan) the day before experiments were performed and incubated at 37 °C and 5% CO_2 overnight. Prior to Raman measurements, cells were rinsed twice with phosphate-buffered saline (PBS; Nacalai Tesque, Japan) at 37 °C and then covered with 2 mL of PBS supplemented with glucose and $MgCl_2$ (both from Nacalai Tesque, Inc., Japan) at 37 °C before being transferred to the Raman microscope for measurement. Considering batch effects that may occur on a dish-to-dish or day-to-day level, multiple cell preparations were measured on different days. A summary of the measurement schedule and cell preparations is given in Table S1.

https://doi.org/10.1021/acs.analchem.4c00236
Anal. Chem. 2024, 96, 7047−7055

Raman Spectroscopy. Raman measurements were performed by using a Raman-11 (Nanophoton, Japan) system with 532 nm excitation with a 1.0 NA CFI Apo 60× NIR water immersion objective (Nikon, Japan). Spectra were measured by a spectrograph with a 600 g/mm grating, using a PIXIS 400 (Princeton Instruments) camera with a 1340 × 400 pixel array of $20 \times 20\ \mu m^2$ pixels, resulting in a 530−2981 cm^{-1} spectral range. Raman measurements were taken using four different measurement regimes, as summarized in Figure 1. For full imaging, the microscope was operated in line scanning mode (where the laser point is rapidly scanned to form a pseudoline) with the width for the scan (x-dimension) set to 100 pixels (equivalent to 35.56 μm) and the height of the image (y-dimension) determined by the size of the cell. For line skip imaging, images were recorded using line scanning mode with the width set to 100 pixels, but the height set to 20 pixels, rather than the full cell, and only every second line in this region recorded (resulting in a 100 × 10 pixel final image). For spatially averaged measurements, Raman spectra were recorded in single-point mode, but with the sample held in a stage scanner (described in the next section), to allow the cell to be moved continuously by approximately 20 μm during the measurement. Finally, for single-point measurements, the microscope was operated in point mode and spectra were recorded from three places in each cell—in the nucleus, at the cytoplasm−nucleus boundary, and within the bulk of the cytoplasm (positions determined by cellular contrast in the visible microscopy images). Across these four different modalities, there is a considerable range in the measurement times needed, with imaging measurements requiring considerably more time than the single-point modes. For measurements investigating the effect of exposure time, spectra were recorded at 100 mW (at the sample) with 1, 3, 5, or 7 s exposure per line or spectrum for imaging/single-point measurements, respectively. For the measurements investigating laser power, the exposure time was set at 3 s and measurements were taken with laser powers of 30, 50, 100, 150, or 200 mW at the sample. For experiments evaluating whether the measurement itself can cause an effect, a second measurement was taken with identical conditions immediately after the first. These sequential pairs were acquired ten times for each of the conditions to assess whether our method for evaluating repeatability was itself repeatable or not.

Stage Scanning Device. Spatially averaged measurements are typically achieved by either (1) by control of the laser position during Raman acquisition[5] or (2) by motorized stage to scan the target cell during the single-point acquisition. Many Raman systems are not freely customizable to control the beam during acquisition, and we constructed a simple stage scanner in order to oscillate the sample and spatially average the spectra during the measurement. Using two small speakers and a three-dimensional (3D) printed mount, the compact stagetop device can oscillate a 35 mm dish at an amplitude of ∼20 μm at frequencies of around 100 Hz, allowing for spatially averaged measurements from what would otherwise be a static single-point measurement. This device can, in principle, be used on any upright/inverted microscope. Further details are in the Supporting Information (Figure S1).

Data Extraction. Raman data was extracted from the recorded measurements in slightly different ways depending on the measurement mode. An overview is given in Figure 1 (bottom row; extracted data regions are identified in red). Although imaging modes produce multiple pixels each containing spectral information, for this comparison, we merged pixel data from a rectangular region into a single spectrum for each cell. Due to differing cell sizes, the rectangular box used to map out the internal cell area for data extraction had a range of different sizes (for Raw 264.7 cells, each side was between 21 and 42 pixels and was significantly more for the larger MEF cells between 41 and 191 pixels). Similarly, for line skip images, data analysis was performed on a single spectrum averaged from a subregion 10 pixels in the y-dimension and either 40 pixels (for Raw 264.7 cells) or 90 pixels (for MEF cells). The spectra obtained from the spatially averaged measurements are a single spectrum per cell/condition and were therefore used directly for analysis. The single-point measurements without spatial averaging similarly produced one spectrum per cell suitable for further analysis (although we did additionally measure specific locations in order to compare how a targeted single-point measurement might perform).

Spectral Data Processing. Extracted spectra were baseline-corrected using a weighted least-squares baseline algorithm (fourth order) and smoothed (Savitzky-Golay, 5 point window, zero order, and no derivative) using the PLS Toolbox (Eigenvector Research Inc.) operating in Matlab (Mathworks). Spectra were then cropped to remove the silent region (1800−2800 cm^{-1}), leaving the spectral range 530−1800 and 2800−2981 cm^{-1} for subsequent analysis. To calculate differential spectra for each of the paired measurements, the spectrum measured in the second was subtracted from the first. Each of the 10 differential spectra was then averaged to produce a mean differential spectrum for each measurement mode/condition.

Principal Component Analysis−Linear Discriminant Analysis (PCA-LDA). PCA-LDA analysis was performed in Matlab (Mathworks) using scripts written in-house. To quantify the discrimination power of a given Raman mode, PCA-LDA was used on spectra obtained from the first measurement only. (The second measurements from each cell were only used for differential spectra analysis to study possible damage and were not included in the PCA-LDA for cell line discrimination.) Spectra obtained from MEF and Raw 264.7 cells were analyzed together, and data was grouped by measurement mode and category (i.e., laser power or exposure time). All first-measurement spectra from a parameter range were included in each PCA-LDA, i.e., 30−200 mW for power or 1−7 s for exposure. Data dimensionality was reduced by applying PCA to these combined data sets and selecting the first 15 principal components (PCs) with which to reconstruct the data set. LDA was performed on the reconstructed data sets.

RESULTS AND DISCUSSION

Effect of Measurement Parameters on Raman Spectral Content and Quality. Since the range of measurement parameters and modes was so varied, we first checked that the resulting spectra were free from obvious artifacts or poor signal-to-noise ratio across all parameters, as discussed below. The mean uncorrected spectra (no baseline correction, normalization, etc.) obtained for both cell types, and for all measurement modes investigated (Figure S2), show an increase in overall Raman signal intensity as well as background of the Raman spectrum with increasing exposure time and/or laser power. We did not observe significant trends in Raman spectra (such as appearance, disappearance, or shifting of bands) with increasing exposure or laser power for any of the measurement modes. The background signal itself differs slightly, with the imaging modes having a sloped baseline, whereas the single-point-based measurement modes have a flatter baseline. The

https://doi.org/10.1021/acs.analchem.4c00236
Anal. Chem. 2024, 96, 7047−7055

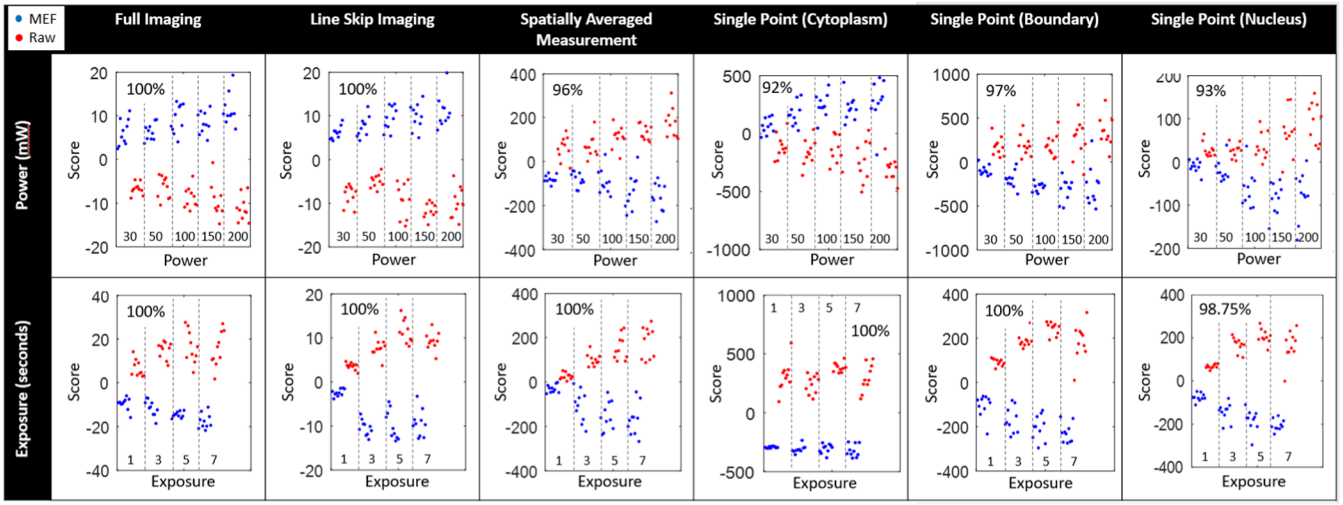

Figure 2. PCA-LDA results assess the discrimination power of spectra from MEF and Raw 264.7 cells for each measurement mode. Top row: Single-cell discrimination at various laser powers (powers denoted on the horizontal axis in mW). Bottom row: Single-cell discrimination at various exposure times denoted on the horizontal axis in seconds. MEF cells are represented by blue dots and Raw 264.7 cells are represented by red dots. Dotted lines separate each of the power/exposure settings, the values of which are shown at the bottom of each panel. Percentages shown are the accuracy of training classification for the data shown in each panel.

spectral profile varies between the imaging and single-point modes, with the spectra obtained with the imaging modes containing a number of bands originating from the quartz substrate[18] (e.g., the broad bands between 750−850 and 1050−1080 cm^{-1}), which are not as distinct in the spectra obtained with single-point-based measurement modes. Conversely, there are a number of bands, particularly the phenylalanine band[19] at ∼1004 cm^{-1}, that appear sharper/more distinct in the single-point-based measurements.

As expected, individual spectra exhibit significant variation (Figure S3). The greatest amount of variation between the 10 spectra recorded at the same conditions is seen for single-point spectra, where the laser only probes a small section of the cell, so that the Raman spectra are strongly influenced by local distributions of molecules within the cell. For the spatially averaged measurements, the Raman band profile is less affected by the local distribution of molecules within the cell, since the Raman signal is obtained from a wider region of the cell than for the conventional single-point spectra. However, as a consequence of spatially scanning during the acquisition, the total path incorporates a wider area during the exposure and is less able to bleach away autofluorescent molecules. In contrast, for single-point measurements, where the laser position remains stationary for the entire measurement, autofluorescence present at the focal spot is more rapidly bleached early during the measurement time frame and is then less apparent in the spectra. Spectra recorded using imaging modes that were then averaged to a single-cell characteristic spectrum show much less variation between measurements than those recorded using single-point-based methods. This is due to the fact that the imaging spectra are already averaging a large number of pixels, as well as covering a large region of the cells.

In order to more directly assess the usefulness of these spectra measured in the different modes and thereby compare the modes, PCA-LDA was performed in order to assess the discrimination potential for the MEF and Raw 264.7 spectra (Figure 2). For full imaging and line skip imaging, for both power- and exposure-based measurements, the two cell type spectra are easily distinguishable from each other even at low laser power or exposure time. This high level of discrimination achieved by the PCA-LDA results from the fact that the imaging modes provide spectra obtained from all or a significant proportion of the cell and therefore contain contributions from nearly all molecules within the cell. For the spatially averaged measurements and the single-point spectra, there is more overlap between the two spectral groups, with the discrimination ability improving slightly with laser power and more significantly with exposure time. Although the single-point results shown in Figure 2 show reasonably good separation between the two spectral groups, particularly at higher laser power or exposure time, this is particularly dependent on the position in the cell that the spectra were collected from. The PCA-LDA performed on single-point data taken at the cytoplasm−nucleus boundary shows an improved discrimination compared to cytoplasm or nucleus measurements. This is likely because (1) the cytoplasm−nucleus boundary contains a more characteristic mixture of all molecules in the cell compared to either region alone and (2) in order to measure the boundary location, it must be first identified and then targeted so that boundary measurements are fundamentally less random than single points usually measured in a cell. The spatially averaged spectra, which contain information from both the cytoplasm and the nucleus, show similar performance to the single-point spectra taken from the boundary region but do not require intervention and specific targeting and are therefore more suitable for high-throughput single-cell analysis.

Effect of Measurement Parameters on Cell Health/Damage. In order to assess the impact of a Raman measurement on the cells, we performed sequential measurements, resulting in two spectra for each cell, with the second spectrum recorded immediately after the first. The resulting differential spectra are displayed in Figure 3 (full imaging and line skip imaging) and Figure 4 (spatially averaged and single-point measurements). Since experimentally measured spectra always contain random amounts of noise, sequential spectra will not be identical, even if the Raman measurement itself causes no change in the sample. Any effects of the laser irradiation may

https://doi.org/10.1021/acs.analchem.4c00236
Anal. Chem. 2024, 96, 7047−7055

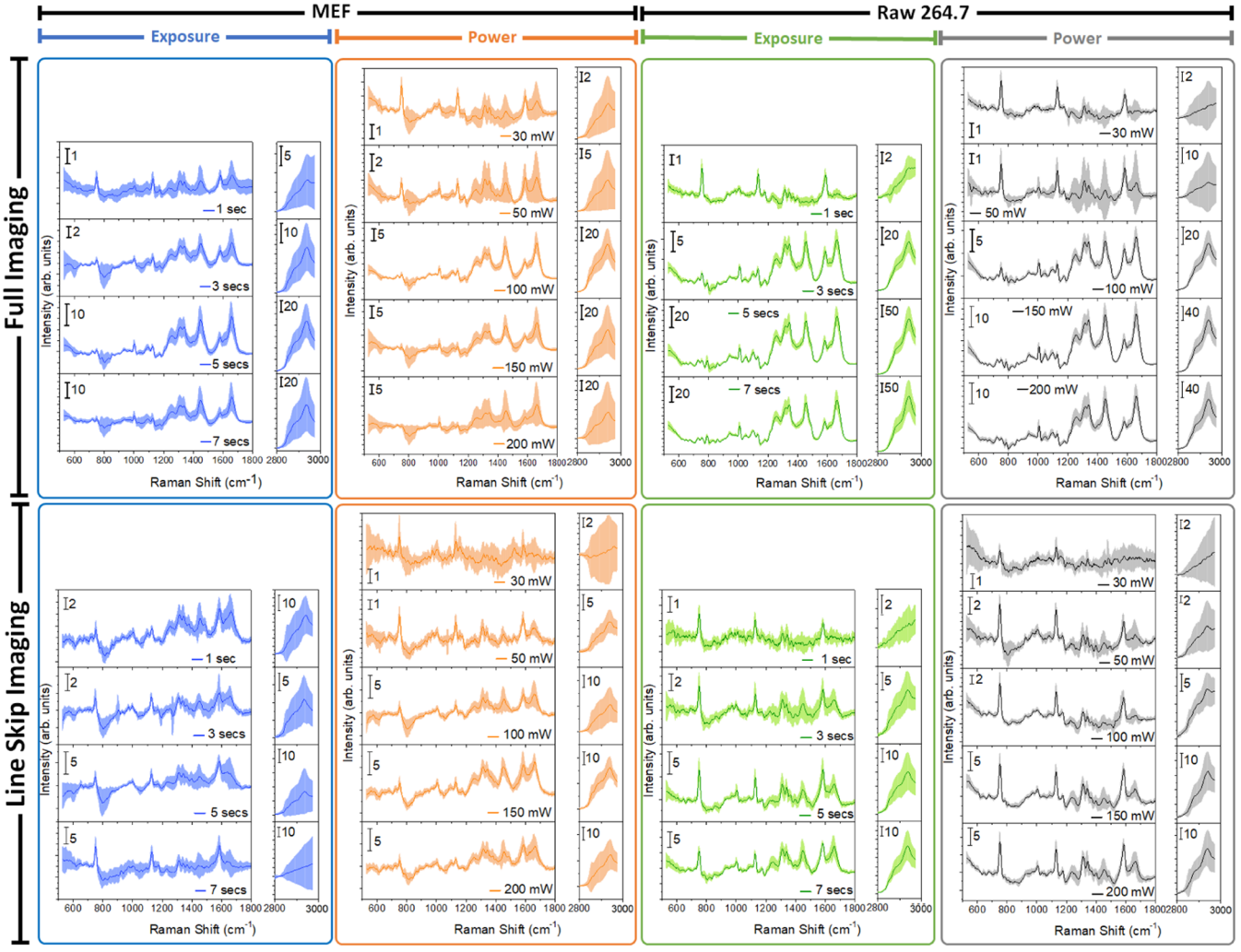

Figure 3. Mean differential spectra (obtained from subtracting the second measured spectrum from the first measured spectrum for the 10 paired measurements) for different imaging modes with full imaging measurements (top) and line skip imaging measurements (bottom). The panels show the mean differential spectra for each power and exposure time investigated and the shading represents ±1 standard deviation. MEF cell measurements are shown in blue (for exposure times) and orange (for laser power). Raw 264.7 cell measurements are shown in green (for exposure times) and gray (for laser power).

then appear in the differential spectra, potentially affecting repeatability, intensity, and spectral profile.

Comparison of the measurements taken at each exposure time and laser power shows that under full imaging (Figure 3), a change occurs with parameters between 1 and 3 s and between 50 and 100 mW for both cell types. The mean differential spectra obtained at 1 s exposure and at 30 and 50 mW show profiles that contain prominent bands from cytochromes[20,21] at 749, 1129, 1313, and 1585 cm^{-1}, particularly clear in the Raw 264.7 cell spectra, along with some bands originating from a range of other cellular materials, such as proteins present at ~1664 cm^{-1}.[19,22] The standard deviation, shown by the shading either side of the mean spectra, shows a relatively broad spread at these low exposure times/laser powers, indicating that for the 10 measurements taken, the second spectrum is sometimes more intense than the first, and vice versa. At longer exposures and/or laser powers, the mean differential spectra no longer show significant contributions from cytochromes and instead show a profile similar overall to that of a cell, swamping the cytochrome bands. From the standard deviation, we can see that a consistent difference emerges, with the second measurement having a lower intensity than that of the first.

From the spectral profiles, it is clear that these differences cannot be explained only by a change in background fluorescence but result from a more fundamental effect of the measurement process on the cellular spectra. Finally, mean differential spectra from MEF cells often show a negative band close to 800 cm^{-1}, likely to originate from the quartz substrate the cells are attached to, supporting the finding that the second measured spectra are weaker than the first.

Full image measurements often resulted in visible damage to the cells after the first measurement (Table 1). Raw 264.7 cells appear to be more susceptible to damage than MEF cells at the same measurement parameters, presumably because a larger area of the Raw 264.7 cells was exposed to the laser (the x-dimension was fixed to 100 pixels, so for Raw 264.7 cells, the entire width of the cell would be exposed, whereas for MEF cells that were typically wider than 100 pixels, only a portion of the cell would be exposed). For both cell types, the mean spectral intensity (Figure S4) increases with exposure time or laser

https://doi.org/10.1021/acs.analchem.4c00236
Anal. Chem. 2024, 96, 7047−7055

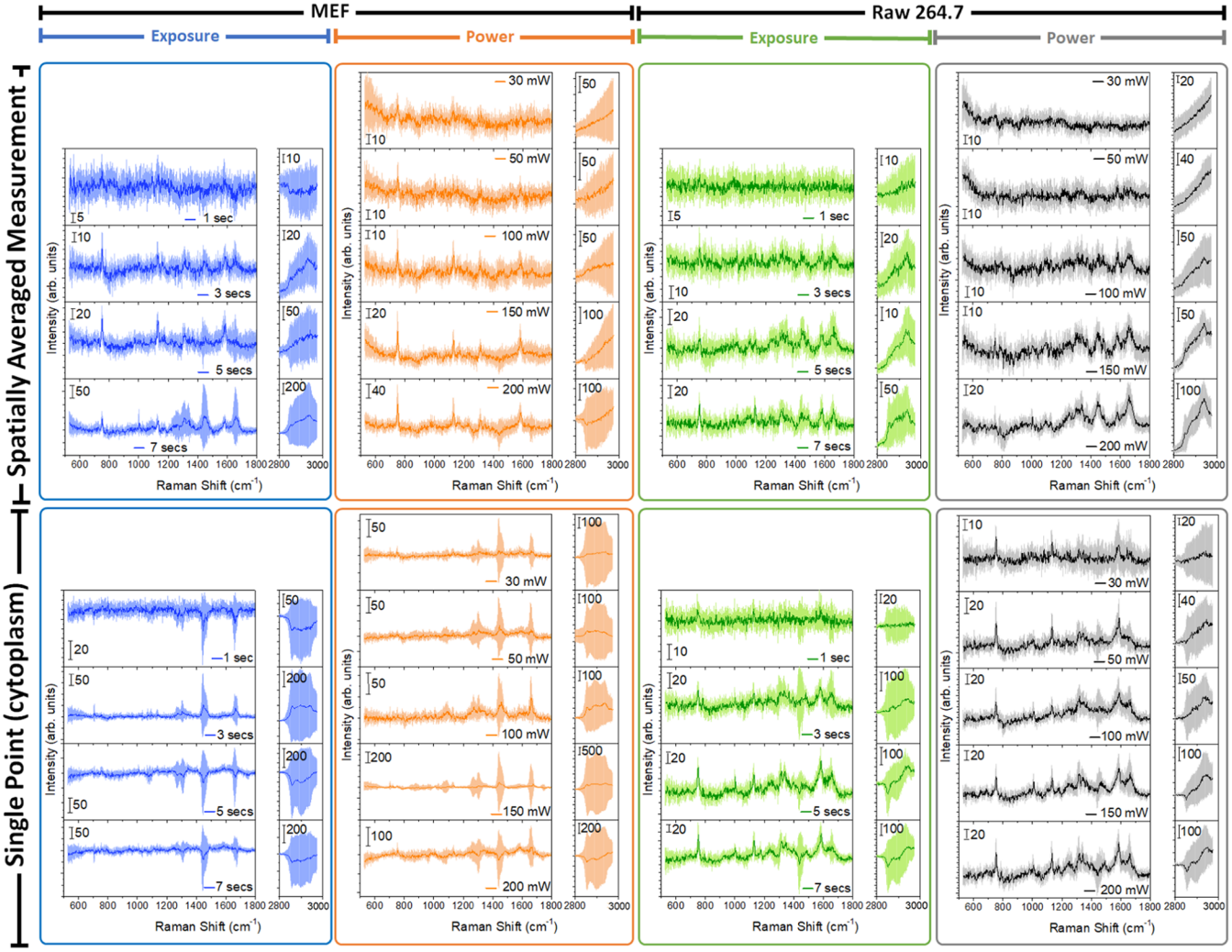

Figure 4. Mean differential spectra (obtained from subtracting the second measured spectrum from the first measured spectrum for the 10 paired measurements) from different point modes, with spatially averaged measurements (top) and single-point cytosolic measurements (bottom). The panels show the mean differential spectra for each power and exposure time investigated and the shading represents ±1 standard deviation. MEF cell measurements are shown in blue (for exposure times) and orange (for laser power). Raw 264.7 cell measurements are shown in green (for exposure times) and gray (for laser power).

Table 1. Number of MEF and Raw 264.7 Cells from 10 Replicates Showing Visible Signs of Damage after Initial Raman Measurement for Each Measurement Mode

		full imaging		line skip imaging		spatially averaged		single point	
		MEF	raw	MEF	raw	MEF	raw	MEF	raw
power	30 mW	1	0	0	0	0	1	0	0
	50 mW	1	1	0	1	0	0	0	0
	100 mW	3	3	0	1	0	0	0	0
	150 mW	4	6	0	0	0	0	0	0
	200 mW	5	8	0	1	0	0	0	0
exposure	1 s	0	0	0	0	0	0	0	0
	3 s	0	1	0	0	0	0	0	0
	5 s	1	10	0	1	0	1	0	0
	7 s	4	10	0	1	0	0	0	0

power, reaching a peak at 5 s or 150 mW, before decreasing slightly for measurements taken at 7 s or 200 mW exposure.

Subsampling by line skip imaging appears to be much less visibly damaging than full imaging, with fewer cells showing signs of blebbing. The mean spectral intensity (Figure S4) is also much lower than in full imaging, again suggesting that line skip imaging induces less change in the cells being measured. Mean differential spectra for line skip measurements (Figure 3) taken at lower laser powers suggest relatively little change is induced under these conditions. As exposure time or laser power increases, the signal-to-noise ratio of the differential spectra increases, as the effect of the measurement itself begins to

https://doi.org/10.1021/acs.analchem.4c00236
Anal. Chem. 2024, 96, 7047−7055

become evident. In the case of line skip imaging, the main contributions to the mean differential spectra are from cytochromes,[20,21] particularly for Raw 264.7 cells, where it is observed at all exposure times and laser powers. Overall for both cell types, this suggests that the line skip imaging measurements have a less severe impact on the measured cells compared to full imaging.

Raman measurements taken by the spatially averaged measurement mode showed visible signs of cell damage in only a small number of cells, and these did not appear to be directly related to increased exposure time or laser power. The mean spectral intensity (Figure S4) is relatively low for both cell lines and all spatially averaged measurements. The mean differential spectra (Figure 4, top panel) are noisy in profile and low in intensity, indicating that there is a small amount of spectral change between the first and second measurements. Notable spectral features, which may indicate measurable cell changes induced by the first Raman measurement, emerge only at higher exposure times (3 s and above) or higher laser powers (100 mW and above). Here, weak Raman bands at ∼1319, 1342, 1456, and 1664 cm^{-1} consistent with proteins[19,22,23] are observed in the Raw 264.7 mean differential spectra with some cytochrome bands present in the mean differential spectra from the MEF cells.

When using the conventional single-point mode (without spatial averaging), no visible cell damage or cellular changes were observed for the parameters used here. As can be seen from the low mean spectral intensity and high standard deviation for cytoplasm-based measurements (Figure S4), the measurement itself does not induce significant change in the sample. This relatively small variation is also shown in the mean differential spectrum (Figure 4, bottom panel). As exposure time or laser power is increased, some consistent Raman features also begin to emerge, namely, cytochromes and weak protein contributions for Raw 264.7 cell measurements, but these do not have such distinct profiles as seen for either of the imaging measurement modes. A similar pattern is seen for MEF measurements taken under different exposure times, with a few weak features originating from cell molecules observed in the mean differential spectra recorded at 5 or 7 s exposure. However, for a small region of the cell, molecules are expected to move in and out of the measurement region during the exposure time. The main features of interest in the mean differential spectra are a series of relatively narrow Raman bands at ∼1270, 1308, 1446, and 1662 cm^{-1}, which would be consistent with the presence of unsaturated fatty acids.[24,25] Therefore, the molecules moving in or out of the measurement region are lipid-based, possibly within membranes or, more likely, due to the large changes in band intensity from lipid droplets or similar structures in the cytoplasm. Further evidence that these lipid-based changes arise from the cytoplasm contributions to these boundary measurements comes from analyses of single-point measurements taken in the cytoplasm−nucleus boundary (Figure S5, top panel) that shows similar lipid-based features, which are not observed in the nucleus (Figure S5, bottom panel).

CONCLUSIONS

For all measurement modes investigated, increasing the laser power or exposure time should lead to more intense spectra with greater definition of Raman bands at higher power or exposure. These expectations are borne out overall in the results. Increasing the laser power or exposure time beyond what is needed for the target of the study, however, comes at the cost of increasing measurement time as well as significantly increasing the risk of cell damage (as defined by visible damage to the cell, summarized in Table 1). In addition to visible damage, higher laser power or exposure times showed consistent differences in the spectral content when compared across sequential measurements. These spectral differences (most notably shown in this work as mean differential spectra) are attributable to a wide range of cellular molecules and generally indicate a loss of cellular signal from the region of interest after the first measurement has been recorded. At lower exposure and laser power, a small but consistently detectable effect (i.e., difference between sequential measurements) was still observed and, by analysis of the peaks, appeared to be largely confined to cytochrome-based changes, suggesting that these are the first molecular changes, which occur as a result of the measurement process. While it is not surprising that the results show that full imaging measurements should be performed at minimal laser power and/or exposure times, perhaps less obvious is the implication that care should be taken when assigning biological significance to bands, especially in relation to cytochromes.

When restricting the amount of exposure by line skip imaging, the amount of time required to image a cell can be reduced, thereby reducing the risk of sample damage, even at higher laser power and exposure times, when compared with full imaging. This is also reflected in the differential spectra observed between the sequential measurements. While the mean differential spectra suggest that line skip imaging has less impact on the cells being measured, the PCA-LDA-based cell line discrimination shows that line skip imaging can still effectively discriminate between cell types, even at low laser power or short exposure times. Despite the significant reduction in measurement time, line skip measurements still provide an ability to discriminate cell types comparable to that of full imaging.

Both spatially averaged and single-point measurements are particularly beneficial, where single-cell heterogeneity is investigated since the short measurement times allow for a much greater number of cells to be measured compared to imaging modes. The PCA-LDA performance of single-point measurements is dependent on the subcellular location of the measurements. Those taken exclusively from the cytoplasm or the nucleus have slightly lower performance than those taken from the cytoplasm−nucleus boundary. However, it should be noted that these boundary-based measurements are the "best case" scenario for single-point measurements, having been hand-selected, which is not feasible for many studies. In addition, the mean differential spectra show that single-point measurements exhibit large profile changes. While we cannot rule out that some of these differences may result from the measurement itself, the data suggest that significant internal movement of organelles/biomolecules within the cell are responsible.

The mean differential spectra obtained for spatially averaged measurements show the least effect of the measurement itself for any of the four modes discussed here. Although some cellular changes are observed at higher laser power and exposure time, spatially averaged measurements with laser powers up to 100 mW and exposure times of up to 3 s show no significant impact from the measurement. This means the data from which the PCA-LDA model is built contains cellular information from regimes, where no cell damage is evident, as well as from higher power/exposure measurements, where some degree of laser-induced damage can be expected. The possibility for individual cell types to respond differently at higher laser power/exposure

https://doi.org/10.1021/acs.analchem.4c00236
Anal. Chem. 2024, 96, 7047−7055

does exist, although the clear separation at low laser power/exposure indicates that the classification ability of the measurement is not dominated by laser-induced change. These results suggest that the trade-off between throughput and separation ability (as determined by PCA-LDA) can be relatively freely optimized, with clear separation across a wide range of laser parameters, including those with and without laser-induced change, although obviously any laser-induced change should ideally be avoided. Out of the higher-throughput methods presented here, the spatially averaged mode compares favorably to optimized single-point measurements taken at the cytoplasm−nucleus boundary and outperforms those taken in the cytoplasm or nucleus, suggesting that it would also outperform a more typical measurement approach targeting a somewhat random location in the cell. In addition, spatially averaged measurements are less susceptible to local movement of biomolecules compared to single-point spectra, as they are generated from a larger region of the cell than conventional single-point measurements. As such, spatially averaged measurements can be a good choice for studies, where large numbers of samples should be measured, where subcellular spatial information is not required and/or where sequential measurements of the same cell (e.g., studies of cell changes over time) are required.

■ ASSOCIATED CONTENT

Supporting Information

The Supporting Information is available free of charge at https://pubs.acs.org/doi/10.1021/acs.analchem.4c00236.

Schedule of Raman measurements recorded for this study (Table S1); stage scanning device and graphical representation of the scanning pattern used for the spatially averaged measurements (Figure S1); average spectra obtained from MEF and Raw 264.7 cells for each measurement mode (Figure S2); assessment of spectral variability for MEF cell measurements at 100 mW and 3 s exposure for each measurement mode (Figure S3); assessment of overall spectral differences between sequential measurements taken with each measurement mode (Figure S4); and assessment of spectral differences between two sequential measurements for single-point measurements taken from the cytoplasm−nucleus boundary and the nucleus only (Figure S5) (PDF)

■ AUTHOR INFORMATION

Corresponding Authors

Alison J. Hobro − *Biophotonics Laboratory, Immunology Frontier Research Center, Osaka University, Suita City, Osaka 565-0871, Japan;* orcid.org/0000-0002-8285-0919; Email: ajhobro@ifrec.osaka-u.ac.jp

Nicholas I. Smith − *Biophotonics Laboratory, Immunology Frontier Research Center, Osaka University, Suita City, Osaka 565-0871, Japan; Center for Infectious Disease Education and Research (CIDER), Suita City, Osaka 565-0871, Japan; Open and Transdisciplinary Research Institute (OTRI), Suita City, Osaka 565-0871, Japan*; Email: nsmith@ap.eng.osaka-u.ac.jp

Authors

Nicolas Pavillon − *Biophotonics Laboratory, Immunology Frontier Research Center, Osaka University, Suita City, Osaka 565-0871, Japan;* orcid.org/0000-0003-2606-2675

Kota Koike − *Nanophotonics Laboratory, Department of Applied Physics, Graduate School of Engineering, Osaka University, Suita City, Osaka 565-0871, Japan*

Takeshi Sugiyama − *Nano-spectroscopy Laboratory, Department of Applied Physics, Graduate School of Engineering, Osaka University, Suita City, Osaka 565-0871, Japan*

Takayuki Umakoshi − *Nano-spectroscopy Laboratory, Department of Applied Physics, Graduate School of Engineering, Osaka University, Suita City, Osaka 565-0871, Japan;* orcid.org/0000-0002-0479-1124

Prabhat Verma − *Nano-spectroscopy Laboratory, Department of Applied Physics, Graduate School of Engineering, Osaka University, Suita City, Osaka 565-0871, Japan;* orcid.org/0000-0002-7781-418X

Katsumasa Fujita − *Nanophotonics Laboratory, Department of Applied Physics, Graduate School of Engineering, Osaka University, Suita City, Osaka 565-0871, Japan;* orcid.org/0000-0002-2284-375X

Complete contact information is available at: https://pubs.acs.org/10.1021/acs.analchem.4c00236

Author Contributions

This manuscript was written through contributions of all authors.

Notes

The authors declare no competing financial interest.

■ ACKNOWLEDGMENTS

This work was funded by the Japan Society for the Promotion of Science (JSPS) through the Funding Program for World-Leading Innovative R&D on Science and Technology (FIRST Program); the JSPS World Premier International Research Center Initiative Funding Program; and the Uehara Memorial Foundation.

■ REFERENCES

(1) Puppels, G. J.; de Mul, F. F. M.; Otto, C.; Greve, J.; Robert-Nicoud, M.; Arndt-Jovin, D. J.; Jovin, T. M. *Nature* **1990**, *347* (6290), 301−303.

(2) Palonpon, A. F.; Ando, J.; Yamakoshi, H.; Dodo, K.; Sodeoka, M.; Kawata, S.; Fujita, K. *Nat. Protoc.* **2013**, *8* (4), 677−692.

(3) Kashima, Y.; Sakamoto, Y.; Kaneko, K.; Seki, M.; Suzuki, Y.; Suzuki, A. *Exp. Mol. Med.* **2020**, *52* (9), 1419−1427.

(4) Pavillon, N.; Smith, N. I. *Opt. Express* **2016**, *24* (26), 30038.

(5) Pavillon, N.; Smith, N. I. *J. Biomed. Opt.* **2015**, *20* (1), No. 016007.

(6) Shin, K.; Chung, H. *Analyst* **2013**, *138* (12), 3335−3346.

(7) Zhao, Z.; Chen, C.; Xiong, H.; Ji, J.; Min, W. *Anal. Chem.* **2020**, *92* (14), 9603−9612.

(8) König, K.; Riemann, I.; Fischer, P.; Halbhuber, K. J. *Cell. Mol. Biol.* **1999**, *45* (2), 195−201.

(9) Chung, S. H.; Mazur, E. *J. Biophotonics* **2009**, *2* (10), 557−572.

(10) Lapotko, D. O.; Zharov, V. P. *Lasers Surg. Med.* **2005**, *36* (1), 22−30.

(11) Smith, N. I.; Fujita, K.; Kaneko, T.; Katoh, K.; Nakamura, O.; Kawata, S.; Takamatsu, T. *Appl. Phys. Lett.* **2001**, *79* (8), 1208−1210.

(12) Kilian, N.; Goryaynov, A.; Lessard, M. D.; Hooker, G.; Toomre, D.; Rothman, J. E.; Bewersdorf, J. *Nat. Methods* **2018**, *15* (10), 755−756.

(13) Bora, K.; Kumar, B.; Prakash, S.; Rathi, A. *J. Biophotonics* **2019**, *12* (10), 1−11.

(14) Tulsawani, R.; Sharma, P.; Sethy, N. K.; Kumari, P.; Ganju, L.; Prakash, S.; Chouhan, S. *PLoS One* **2020**, *15* (3), No. e0230175.

(15) Magidson, V.; Khodjakov, A. Circumventing Photodamage in Live-Cell Microscopy. *Methods in Cell Biology*; Elsevier Inc., 2013; Vol. *114*, pp 545−560.
(16) Schilling, Z.; Frank, E.; Magidson, V.; Wason, J.; Loncarek, J.; Boyer, K.; Wen, J.; Khodjakov, A. *J. Microsc.* **2012**, *246* (2), 160−167.
(17) Li, B.; Larkin, P. J. *Appl. Spectrosc.* **2020**, *74* (7), 741−750.
(18) Tobin, M. C.; Baak, T. *J. Opt. Soc. Am.* **1968**, *58* (11), 1459−1461.
(19) De Gelder, J.; De Gussem, K.; Vandenabeele, P.; Moens, L. *J. Raman Spectrosc.* **2007**, *38* (9), 1133−1147.
(20) Spiro, T. G.; Strekas, T. C. *Proc. Natl. Acad. Sci. U.S.A.* **1972**, *69* (9), 2622−2626.
(21) Hu, S.; Morris, I. K.; Singh, J. P.; Smith, K. M.; Spiro, T. G. *J. Am. Chem. Soc.* **1993**, *115* (26), 12446−12458.
(22) Ashton, L.; Blanch, E. W. *J. Mol. Struct.* **2010**, *974* (1−3), 132−138.
(23) Maiti, N. C.; Apetri, M. M.; Zagorski, M. G.; Carey, P. R.; Anderson, V. E. *J. Am. Chem. Soc.* **2004**, *126* (8), 2399−2408.
(24) van Manen, H.-J.; Kraan, Y. M.; Roos, D.; Otto, C. *Proc. Natl. Acad. Sci. U.S.A.* **2005**, *102* (29), 10159−10164.
(25) Sugiyama, T.; Hobro, A. J.; Pavillon, N.; Umakoshi, T.; Verma, P.; Smith, N. *Analyst* **2021**, *146* (4), 1268−1280.

https://doi.org/10.1021/acs.analchem.4c00236
Anal. Chem. 2024, 96, 7047−7055